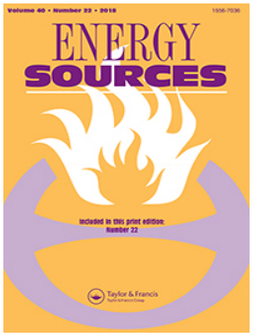

Taylor & Francis
Taylor & Francis Group

Energy Sources, Part A: Recovery, Utilization, and Environmental Effects

ISSN: 1556-7036 (Print) 1556-7230 (Online) Journal homepage: https://www.tandfonline.com/loi/ueso20

Determination of kinetic parameters and thermodynamic properties for ash (Fraxinus) wood sawdust slow pyrolysis by thermogravimetric analysis

Antony Nyombi, Mike Williams & Roland Wessling

To cite this article: Antony Nyombi, Mike Williams & Roland Wessling (2018) Determination of kinetic parameters and thermodynamic properties for ash (Fraxinus) wood sawdust slow pyrolysis by thermogravimetric analysis, Energy Sources, Part A: Recovery, Utilization, and Environmental Effects, 40:22, 2660-2670, DOI: 10.1080/15567036.2018.1502846

To link to this article: https://doi.org/10.1080/15567036.2018.1502846

Published online: 15 Aug 2018.

ENERGY SOURCES, PART A: RECOVERY, UTILIZATION, AND ENVIRONMENTAL EFFECTS
2018, VOL. 40, NO. 22, 2660–2670
https://doi.org/10.1080/15567036.2018.1502846

Taylor & Francis
Taylor & Francis Group

Determination of kinetic parameters and thermodynamic properties for ash (Fraxinus) wood sawdust slow pyrolysis by thermogravimetric analysis

Antony Nyombi[a], Mike Williams[b], and Roland Wessling[a]

[a]Cranfield Forensic Institute, Defence Academy of the United Kingdom, Cranfield University, Shrivenham, UK; [b]Center for Defence Chemistry, Defence Academy of the United Kingdom, Cranfield University, Shrivenham, UK

ABSTRACT

Ash (Fraxinus) wood sawdust pyrolysis under nitrogen was conducted using 2, 5, 10, 15, and 20°C/min heating rates. Friedman and Starink methods were used for kinetic analysis while y(α) master plots were used for pyrolysis mechanisms prediction. The mean activation energy were 198 and 202 kJ/mol for Friedman and Starink, respectively. The master plots predicted that the pyrolysis process could be a combination of diffusion, geometrical contraction, nucleation, and reaction order models. The pre-exponential factors were in the range 10^{12} to 10^{19} s^{-1}. Gibbs free energy was 180 −185 kJ/mol. The entropy values were negative up to $\alpha = 0.75$ indicating high orderliness of products relative to reactants but changed to positive at higher conversions implying likely disorderliness of the products compared to reactants. The calorific value of Ash (Fraxinus) wood sawdust was 18.3 MJ/kg.

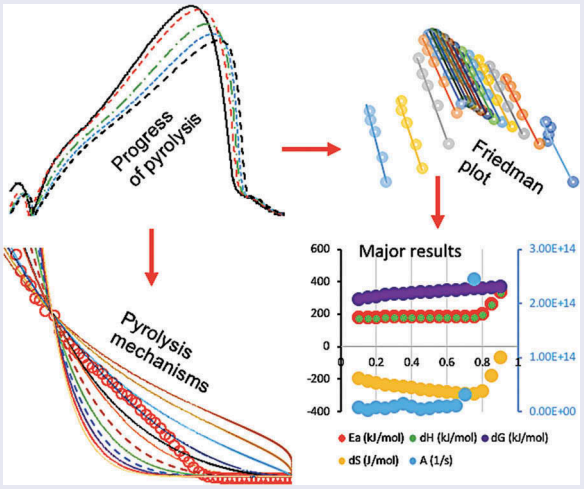

KEYWORDS

Ash (Fraxinus); calorific value; kinetic parameters; slow pyrolysis; thermodynamic properties

Introduction

Energy sources have shifted from biomass to fossil fuels and back to biomass in less than 300 years due to economic and technological developments. The need for renewable sources is on the rise due to their environmental friendliness and sustainability. Globally, 19% of the energy needs are met using renewables, with 9% being contributed by biomass. It is envisaged to increase at a rate of 2.5%

CONTACT Antony Nyombi a.nyombi@cranfield.ac.uk Defence Academy of the UK, Cranfield University, Shrivenham
Color versions of one or more of the figures in the article can be found online at www.tandfonline.com/ueso.

per year (Ahmad et al. 2017). However, investigation of the material properties has to be made to ensure suitability for any probable bioenergy production like biochar. Several researchers have analyzed and characterized a number of biomass resources including beech wood (Ding et al. 2016), pine wood (Mishra, Kumar, and Bhaskar 2015), bamboo (Chen et al. 2015a) among others for their energy potential. Due to the abundant nature of biomass, many materials still remain not fully or uninvestigated, yet they also present enormous potential for bio-oil, biochar, and other useful products.

Pyrolysis and torrefaction (Chen et al. 2015b) are key methods used for processing biomass materials for potential energy production. Thermogravimetric (TG) techniques have been used to study pyrolysis since they are effective and provide a controllable atmosphere and heating rate, with negligible thermal gradients and mass transport (Ding et al. 2016). TG can be used alone or combined with other techniques like spectrometry (Gu et al. 2014) to study biomass materials. The application of TG analysis is appropriate to obtain chemical kinetic parameters, such as activation energy employing differential and integral methods (Wang et al. 2016). However, identifying the appropriate pyrolysis mechanism for processes with changing activation energies across the entire range of conversion requires careful application of model-free and model fitting methods (Vyazovkin et al. 2011). Master plots have been used extensively for predicting pyrolysis mechanisms for biomass pyrolysis (White, James Catallo, and Legendre 2011).

In this study, Ash (Fraxinus) sawdust, material from a perennial plant found in many parts of the world, were investigated. Ash (Fraxinus) trees grow to 40–80 ft tall, are heavily branched and resistant to severe environmental conditions. This study performs characterization and in-depth analysis of Ash (Fraxinus) physiochemical properties, kinetic parameters, thermodynamic properties, and pyrolysis mechanisms. The study highlights the potential application of this plant (material) for energy and the results add to the body of knowledge for biomass materials whose properties are already known.

Methods and materials

Sample preparation and characterization

Sawdust samples from Ash (Fraxinus) tree were ground to fine powder using a laboratory vibratory pulverizer (Essa LM2 pulverizing mill) and sieved to less than 200 μm particle size. They were then further dried in an oven at 105°C prior to storage.

Elemental analysis for carbon, hydrogen, and nitrogen was carried out by the Cranfield University School of Water, Energy and Environment, following British standard BS EN 13654–2:2001 and BS7755, using a Vario EL elemental analyzer. Oxygen levels were determined by difference.

An automated thermogravimetric analyzer (TGA/DSC3+ STAR system – Mettler Toledo, EAG. EID 304 model) was used to measure the moisture content, volatiles, fixed carbon, and ash content as per the D7582-15 standard method. In this method (with slight modifications), approximately 8-mg aliquots of dry sawdust, pulverized to < 200 μm particle size in 70 ml alumina crucibles, were loaded into the TGA instrument and heated in N_2 and air environments at (50/60) ml/s and (25/60) K/s heating rate. For moisture determination, the sample was heated from 303 K to 383 K and held at that temperature for 10 min in N_2. For volatiles, the sample used for moisture was heated further to 1073 K and held at that temperature for 10 min in N_2. For ash, the same sample used for volatiles was heated further at 1073 K for 40 min in air. Fixed carbon (FC) was determined by difference. This procedure was done in triplicate.

The same TGA used for proximate analysis was used for pyrolysis (mass loss determination as a function of temperature and time). Approximately 5 mg of sawdust of less than 210 μm particle size were loaded into 70 ml alumina crucibles and heated at five different heating rates: 2/60, 5/60, 10/60, 15/60, and 20/60 K/s. Samples were heated from 303 K to 1073 K in Nitrogen environment at $(50/60)*10^{-6}$ m^3/s.

Mass loss with temperature and time was recorded automatically. The pyrolysis thermal analysis was done in triplicate.

The calorific value determinations were done at Cranfield University – Bedfordshire campus using the 6400 Automatic Isoperibol Calorimeter. The calorimeter has a precision of 0.1%, temperature resolution of 273.1501 K, calorie sample range of 5000–8000, and a linearity across operating range of 0.05%. The analysis was done in triplicate.

Kinetic properties

The kinetic parameters were determined taking into account the mechanisms for the degradation process of Ash sawdust. The reaction rate is related to the degree of conversion (α) according to Eq. 1 below;

$$\alpha = \frac{M_o - M_i}{M_o - M_\infty} \tag{1}$$

where: M_o, M_i, and $M\infty$ are the initial mass, instantaneous mass, and the final mass. The degradation kinetics (Islam, Asif, and Hameed 2015) can be represented by the expression shown in Eq. 2.

$$\frac{d\alpha}{dt} = k(T)f(\alpha) \tag{2}$$

The temperature dependence of the rate of degradation is related to the Arrhenius Eq. 3:

$$k = A\ exp\left(\frac{-E_a}{RT}\right) \tag{3}$$

where: A, E_a, R, and T are the pre-exponential factor, activation energy, gas constant, and absolute temperature. Substituting Eq. 3 into Eq. 2 gives:

$$\frac{d\alpha}{dt} = A\exp\left(\frac{-E}{RT}\right)f(\alpha) \tag{4}$$

The isoconversional differential method by Friedman and the integral method by Starink were used for determination of activation energy since both are believed to more accurate than similar methods (Starink 2003). These methods take the forms shown in Eqs 5 and 6 respectively.

$$In\left[\beta_k\left(\frac{d\alpha}{dt}\right)_{\alpha,k}\right] = InA_\alpha f(\alpha) - \left(\frac{E_\alpha}{R}\right)\left(\frac{1}{T_{\alpha,k}}\right) \tag{5}$$

$$In\left(\frac{\beta_k}{T_{\alpha,k}^{1.92}}\right) = In\left(\frac{A_\alpha R}{g_{(\alpha)}E_\alpha}\right) - 1.0008\left(\frac{E_\alpha}{R}\right)\left(\frac{1}{T_{\alpha,k}}\right) \tag{6}$$

where:

β_k - kth heating rate,

$T_{\alpha,k}$ - temperature for a given α of k^{th} heating rate,

Ea - apparent activation energy,

A_α - pre-exponential factor of given conversion.

A plot of $In\left[\beta_k\left(\frac{d\alpha}{dt}\right)_{\alpha,k}\right]$ OR $In\left(\frac{\beta_k}{T_{\alpha,k}^{1.92}}\right)$ Vs $\left(\frac{1}{T_{\alpha,k}}\right)$ enables one to estimate Ea from the slopes.

Master plots

The Ea values obtained by the Friedman method were used to determine experimental values for master plots. The approximate constant value of Ea was replaced by the average value $Ea_{(o)}$ that was inserted into the $y(\alpha)$ function, Eq. 7.

$$y(\alpha) = \left(\frac{d\alpha}{dt}\right)_{\alpha,k} \exp\left(\frac{E_{a(o)}}{RT_{\alpha,k}}\right) = \beta_k \left(\frac{d\alpha}{dT}\right)_{\alpha,k} \exp\left(\frac{E_o}{RT_{\alpha,k}}\right) = Af(\alpha) \tag{7}$$

where $d\alpha/dT_{(a,k)}$ is the differential conversion to temperature (T) at given α and a specified heating rate, β, and $E_{a(o)}$ is the mean value of the Ea. The experimental y(α) can be obtained by substituting the $E_{a(o)}$, β_k, R, dα/dT, and T_α into Eq.7. And theoretical y(α) are obtained by substituting the given α into different f(α) described elsewhere (Vlaev et al. 2008). Since the pre-exponential factor (A) of Eq.7 is still unknown, experimental and theoretical y(α) have to be normalized (Vyazovkin et al. 2011), using Eq. 8.

$$y(\alpha)_{norm} = \frac{y(\alpha)}{y(0.5)} \tag{8}$$

Thermodynamic parameters

The thermodynamic parameters including pre-exponential factors (A), enthalpy (ΔH), entropy (ΔS) and Gibbs free energy (ΔG) were calculated from the Eqs. 9–12 (Ahmad et al. 2017).

$$A = .Ea_\alpha \; exp\left(\frac{Ea_\alpha}{RT_m}\right)/R.T_m^2 \tag{9}$$

$$\Delta H = Ea_\alpha - RT \tag{10}$$

$$\Delta G = Ea_\alpha + R.T_m.In\left(\frac{K_b.T_m}{h.A}\right) \tag{11}$$

$$\Delta S = \frac{\Delta H - \Delta G}{T_m} \tag{12}$$

where K_b = 1.38*10^{-23} J/K), h = 6.626*10^{-34} Js), and T_m is the DTG peak temperature.

Results and discussion

Proximate, ultimate, and heating values

Table 1 shows the results for proximate, ultimate, and heating values of raw Ash (Fraxinus) sawdust. These properties, are comparable to and to some extent better than many biomass materials that have

Table 1. Properties of selected materials compared with raw Ash sawdust used in this study.

		Proximate analysis				Ultimate analysis					
Sample	HHV (MJ/kg)	M	V	FC	A	C	H	N	S	O*	Ref.
Ash tree sawdust	18.29	5.66	70.14	21.07	3.13	49.12	6.64	0.35	-	43.89	This study
[a]Ash tree	17.23 –22.06	7.6– 4.2	86.8– 69.3	12.3– 26.1	0.9– 0.4	48.9– 57.3	5.9– 5.8	< 0.1– 0.4	0.2– 0.3	44.9– 36.2	(Haykiri-Acma, Yaman, and Kucukbayrak 2016)
Moso Bamboo	16.85	-	85.53	13.33	1.15	47.58	6.13	0.52	0.04	45.73	(Chen, Zhou, and Zhang 2014)
S. African Coal	27.37	2.70	26.90	56.30	14.10	67.50	4.26	1.76	0.44	11.58	(Wu et al. 2017)

HHV-Higher heating value; *determined by difference; M-moisture content, V-volatile matter, FC-fixed carbon, A-Ash, C-carbon, H-hydrogen, N-nitrogen, S-sulfur, O-oxygen; [a]values were taken before and after torrefaction at 300°C.

been investigated before (Chen, Zhou, and Zhang 2014). Low moisture content allows Ash sawdust to have a rapid heat transfer during pyrolysis (Varma and Mondal 2016) and a high combustion yield. (Singh, Mahanta, and Bora 2017) characterized several biomass materials and found them to have a moisture content of 8.2–13.9wt% which was higher than the 5.7 ± 0.04wt% observed for Ash sawdust. High volatile matter means the material can easily be devolatilized. The ash content was low (3.13 ± 0.02wt%) meaning that devolatilization is not interrupted much and less fouling occurs, little slag formation leading to high thermal efficiency and low operating costs (Peter 2002).

The calorific value of Ash sawdust was 18.29 ± 0.02 MJ/kg in its raw form. This value is higher than that for many other biomass fuels like Moso Bamboo (16.85 MJ/kg) (Chen, Zhou, and Zhang 2014), palm fiber (17.60 MJ/kg), palm sludge (13.80 MJ/kg) (Chong et al. 2017) cotton stalk (15.78 MJ/kg), wheat straw (17.90 MJ/kg), corn stalk (17.79 MJ/kg), vineyard (16.68 MJ/kg), corn cobs (17.99 MJ/kg), sugar beet leaves (17.70 MJ/kg), rice straw (12.13 MJ/kg) (Skoulou and Zabaniotou 2007) but lower than 19.00 MJ/kg for wood reported by (Koyuncu and Pinar 2007). On torrefaction (Daood et al. 2010), Ash sawdust properties were enhanced making it suitable for co-firing or for industrial and domestic settings without any addition of other materials.

Mass loss and conversion

Figure 1A and B shows the mass loss and mass loss rate as a function of temperature. Ash sawdust underwent slow pyrolysis following three major phases. The first phase occurring between 50 and 200°C attributed to the loss of moisture. The second occurred between 200 and 450°C attributed to degradation of hemicellulose and cellulose and the last one occurring between 450 and 800°C (for all heating rates) attributed to degradation of lignin.

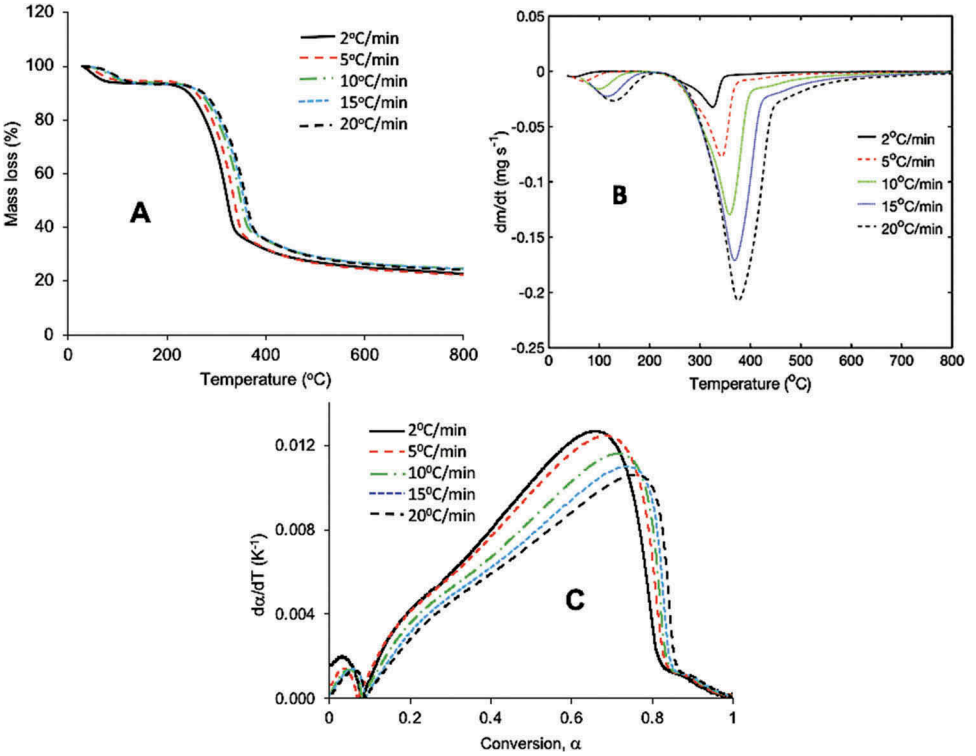

Figure 1. A - Mass loss; B - Mass loss rate; C - dα/dT as a function of conversion.

There is a shift in the attainment of the peak on the mass loss rate graph for each heating rate: 325, 334, 348, 356, and 359°C for 2, 5, 10, 15, and 20°C/min heating rates, respectively.

The hydrophilic nature of sawdust especially the non-crystalline parts and voids allow water molecules to be accommodated in the structure. Sawdust is composed of cellulose (α-cellulose), hemicellulose, lignin, pectin, and waxes with the first three representing up to 99% of sawdust composition. Water is linked to the amorphous region of cellulose through intra- and intermolecular hydrogen bonds on hydroxyl groups and free radicals on cellulose and hemicellulose (Manaila et al. 2016). During phase I (50–200°C), the main event that took place is dehydration of the sawdust. Dehydration reactions are both endothermic and may be reversible involving interface reactions and diffusion. This may involve rapid initial nucleation on the surface followed by an advance of the coherent interface thus formed. Nucleation may be at specific surface sites followed by growth or no growth at all. Structural re-organization leads to the development of cracks, channels or pores through which moisture may escape from the interface (Bamford and Tipper 1980).

In stage II (200–450 °C), the main reactions that take place are the pyrolysis of hemicellulose and cellulose. Hemicellulose is amorphous with a linear framework of xylans and glucomannans. Its conversion takes place mainly in the 200–350°C region catalyzed by mineral matter releasing moisture, CO_2, and other volatiles forming char (Collard and Blin 2014). Cellulose, on the other hand, has both the crystalline and the amorphous phases. The main conversion of cellulose takes place between 300 and 450°C. Decomposition reactions of cellulose at ~ 300°C are responsible for most mass loss as well as the release of CO, CO_2, and other organic compounds.

In the final phase (stage III; 450–800°C), lignin breakdown leads to the formation of pyrolysis gases, and tars which condense on the char wall surfaces (Brebu and Vasile 2010). Several mechanisms describe this region including chemical reactions (Jeguirim et al. 2014), random nucleation and growth, phase boundary mechanisms, and diffusion.

Figure 1C presents the dα/dT as a function of conversion, with a sigmoidal type that is common in linear non-isothermal TGA (Wang et al. 2016) (Khawam and Flanagan 2006). For $0 < \alpha < 0.1$, we observe a prominent peak corresponding to moisture loss. This is followed by a shoulder peak up to $\alpha \sim 0.3$ corresponding to hemicellulose and maximum peak for $0.6 < \alpha < 0.75$ attributed to cellulose decomposition. At $0.85 < \alpha < 1.0$, we observe another shoulder peak corresponding to lignin decomposition reactions. Furthermore, for $0.00 < \alpha < 0.10$ range was related to 50°C < T < 220°C for all heating rates, related to diffusion reactions of moisture through the pores of sawdust. The second conversion range $0.1 < \alpha < 0.8$ corresponded to 180°C < T < 450°C for all heating rates. For $0.80 < \alpha < 1.00$, the main reaction corresponds to lignin breakdown and were within 360 < T < 800°C for all heating rates. We also observe in (Figure 1C), that the derivative dα/dT peak height decreased with increasing heating rate attributed to combined effects of heat and mass transfer within the sample (Wang et al. 2016).

Activation energy

Iso-conversional methods were used for the estimation of activation energies at different degrees of conversion for pyrolysis of Ash (Fraxinus) sawdust. Figure 2A and 2B show the Friedman and Starink plots that were used for calculation of activation energies. These methods gave similar and sensible values at each degree of conversion implying that these methods are appropriate for describing the pyrolysis profile of Ash sawdust. This is further strengthened by the high regression coefficients (0.999) for $0.2 < \alpha < 0.8$, Figure 2C.

The activation energy values obtained could be divided into two main categories; 180–184 (kJ/mol) for $0.1 < \alpha < 0.8$ conversion and 195–350 (kJ/mol) for $\alpha > 0.8$. For $0.1 < \alpha < 0.8$, relatively weak bonds (Toufiq et al. 2013) of hemicellulose and cellulose are being broken. However, for $\alpha > 0.8$ relatively stronger bonds of lignin components are being broken (Islam, Asif, and Hameed 2015), hence, the higher activation energies observed.

The Activation energy (Ea) for Ash (Fraxinus) wood sawdust (198–202 kJ/mol) is similar to waste tea pyrolysis (Ea: 208–223 kJ/mol) (Tian et al. 2016). The results still show that Ash sawdust was not

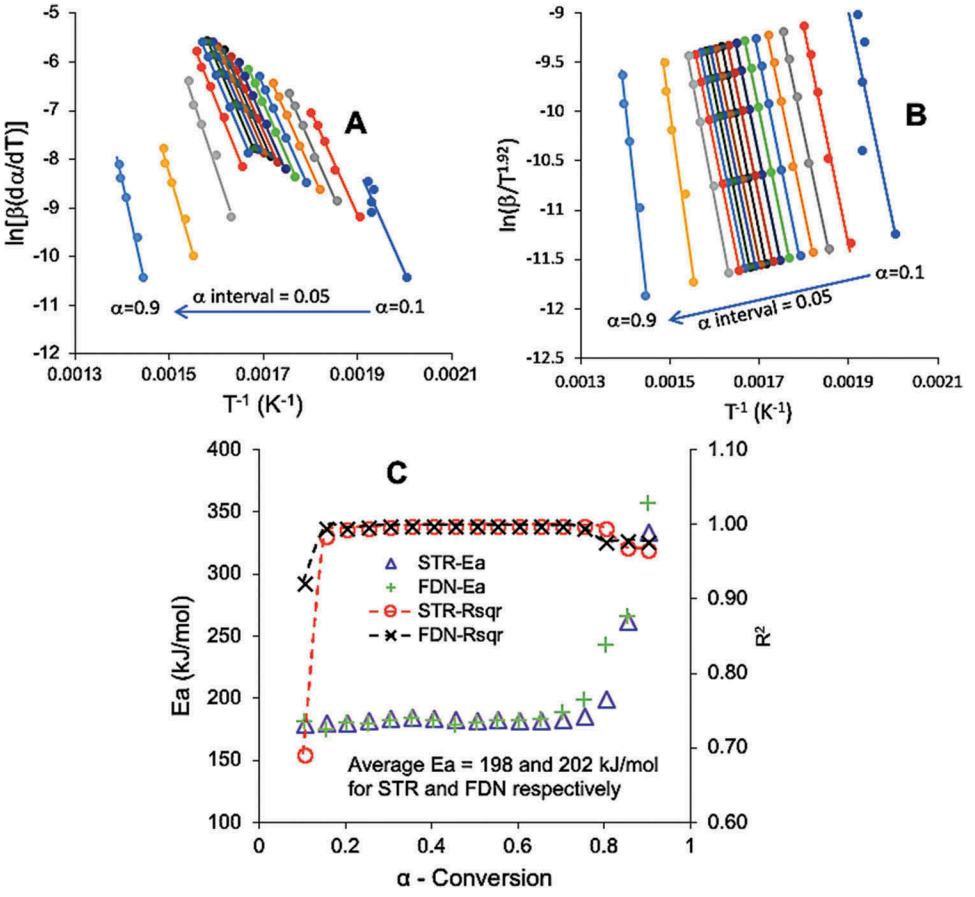

Figure 2. A - Friedman (FDN) plot; B - Starink (STR) plot and C - Activation Energy and regression coefficients for FDN and STR.

so easy to pyrolyse compared to beech wood (Ea: 147-174 kJ/mol) (Ding et al. 2016), moso bamboo (Ea: 96-113 kJ/mol) (Chen, Zhou, and Zhang 2014), and other biomass with lower activation energy (Ceylan, Topcu, and Ceylan 2014) (Ceylan and Topcu 2014) (Slopiecka, Bartocci, and Fantozzi 2012) (Sonobe and Worasuwannarak 2008). However, Ash sawdust pyrolysis seems to be easier to pyrolyse than Corallina pilulifera (Ea: 248 kJ/mol) (Tian et al. 2016), Enteromorpha (Ea: 228 kJ/mol) (Tian et al. 2016), and Rice husks (Ea: 230 kJ/mol) (Tian et al. 2016).

Reaction mechanism prediction using master plots

Vyazovkin *et al.* (Vyazovkin et al. 2011), recommended that when the Ea values obtained vary significantly with conversion, i.e., when the difference between the maximum and minimum values of Ea is more than 20–30% of the average Ea, it is important to integrate over small segments (minimum of α = 0.05 intervals) to avoid systematic errors in Ea.

In this case, the pyrolysis process is multi-step and follows several mechanisms. As seen from Figure 3, the deviations from $E_{a(o)}$ got higher than 30% once the conversion exceeded 0.8 for Starink method and 0.75 for Friedman method. These deviations could be attributed to secondary reactions between the volatiles and char (Wang et al. 2016).

After excluding the Ea values higher than 30% of deviation, $E_{a(o)}$ was calculated from the Friedman method as 184 kJ/mol since differential methods are considered more accurate that

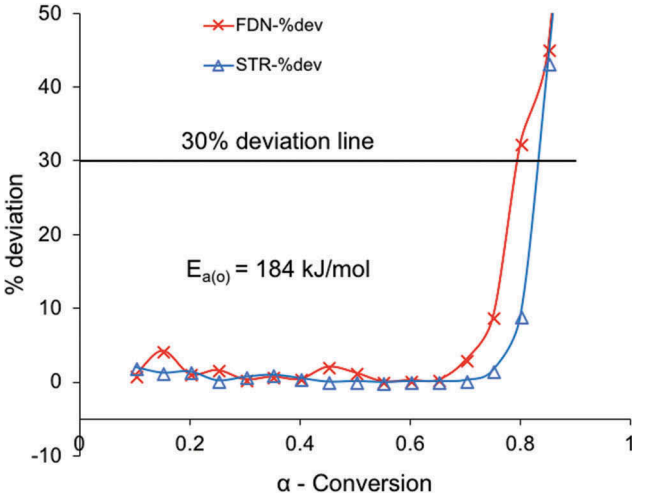

Figure 3. Deviation of Ea from Ea(o).

integral methods (Vyazovkin et al. 2011). As shown in Figure 4A master plots, the experimental y(α) master plot did not fit exactly any of the theoretical master plots. However, Fraxinus pyrolysis plots have a shape similar to "diffusion" especially 5-D at lower conversions (α < 0.5). In the same region, Ash sawdust pyrolysis master plot is similar to and intercepts several reaction order master plots especially n = 2 to n = 8.

At higher conversions (α > 0.5), Ash sawdust pyrolysis master plot resembles the diffusion models D3, and D5 as well as reaction order especially n = 2 for 0.5 < α < 0.75. For α > 0.75, Ash (Fraxinus) master plot pattern follows reaction order mechanisms especially n = 2–9 and still continued to be similar to D5 model Figure 4B. However, the overall pyrolysis process could be a combination of several mechanisms involving diffusion (D3 and D5), geometrical contraction (G2 and G3), reaction order models (n = 2–9) or nucleation (Wang et al. 2016).

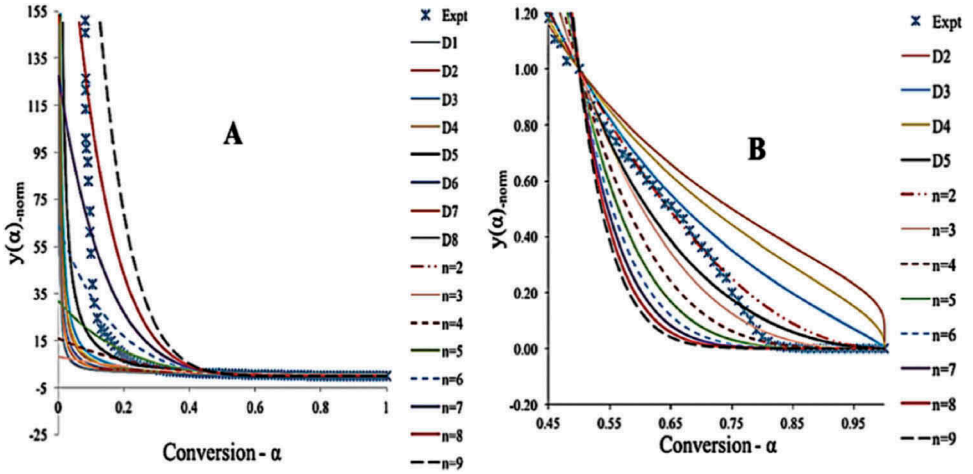

Figure 4. Generalized y(α) master plot (A), and master plot for α >0.45 (B).

Table 2. Thermodynamic parameters for pyrolysis of Ash sawdust.

	Friedman				Starink			
α	A (s^{-1})	ΔH (kJ/mol)	ΔG (kJ/mol)	ΔS (J/mol)	A (s^{-1})	ΔH (kJ/mol)	ΔG (kJ/mol)	ΔS (J/mol)
0.10	7.29E+ 12	176.80	185.29	−13.31	4.95E+ 12	174.80	185.35	−16.53
0.15	2.21E+ 12	170.66	185.48	−23.23	6.52E+ 12	176.22	185.31	−14.25
0.20	6.85E+ 12	176.48	185.30	−13.82	6.10E+ 12	175.88	185.32	−14.80
0.25	5.70E+ 12	175.53	185.33	−15.36	9.37E+ 12	178.09	185.26	−11.23
0.30	8.83E+ 12	177.79	185.27	−11.72	1.37E+ 13	180.04	185.20	−8.09
0.35	1.37E+ 13	180.06	185.20	−8.06	1.49E+ 13	180.50	185.19	−7.35
0.40	8.68E+ 12	177.70	185.27	−11.86	1.28E+ 13	179.69	185.21	−8.66
0.45	4.88E+ 12	174.74	185.35	−16.64	1.06E+ 13	178.75	185.24	−10.17
0.50	6.34E+ 12	176.08	185.32	−14.48	9.80E+ 12	178.33	185.25	−10.85
0.55	9.72E+ 12	178.28	185.25	−10.92	1.01E+ 13	178.46	185.25	−10.64
0.60	9.10E+ 12	177.95	185.26	−11.46	9.72E+ 12	178.29	185.25	−10.92
0.65	1.18E+ 13	179.30	185.22	−9.29	9.77E+ 12	178.31	185.25	−10.88
0.70	3.08E+ 13	184.24	185.08	−1.32	1.17E+ 13	179.23	185.22	−9.40
0.75	2.44E+ 14	194.92	184.79	15.88	1.88E+ 13	181.69	185.15	−5.43
0.80	1.05E+ 18	238.27	183.75	85.45	2.58E+ 14	195.21	184.78	16.34
0.85	9.49E+ 19	261.66	183.27	122.88	4.97E+ 19	258.30	183.33	117.51
0.90	3.52E+ 27	352.57	181.71	267.80	4.51E+ 25	329.80	182.06	231.56

Thermodynamic parameters

The pre-exponential factor (A), enthalpy (ΔH), Gibbs energy (ΔG), and entropy (ΔS) were calculated using Eqs. 9–12. The A values obtained in this study were in the range 10^{12} to 10^{19} except at α > 0.8. ΔG values were constant at 185 kJ/mol and only decrease slightly at α > 0.8 (Table 2).

The values of A for reactions in the solid state vary between 10^{6} to 10^{7} orders of magnitude. Usually, first-order reactions have A in the range of 10^{5} to 10^{18} s^{-1}. Low A values are indicative of surface reactions, but if the reactions are independent of the material surface area, the low A factors would indicate that the activated complex is a 'sophisticated' one, while high A factors indicate a simple complex (Vlaev et al. 2008). Entropy change values obtained had negative values up to α = 0.7 for Freidman and up to α = 0.75 for Starink, indicating that the final products could have been more ordered than the initial reactants (Alves, Maia, and De Morais 2016). The positive entropy values obtained at high conversions indicate that the orderliness of the final products were likely to be less than the original materials (Ch et al. 2008). Furthermore, entropy (ΔS) values are directly related to Ea and A; the higher are the values of Ea and A, the higher are the values of (ΔS) (Vlaev, Georgieva, and Genieva 2007). The occurrence of positive and negative values of (ΔS) shows that the pyrolysis process was complex (Ahmad et al. 2017).

Conclusions

This study investigated the energy values, kinetics, and thermodynamics of Ash (Fraxinus) wood sawdust slow pyrolysis. The activation energy values were 180–350 (kJ/mol). The pyrolysis process could have involved diffusion, geometrical contraction, reaction order models or nucleation. The pre-exponential factors were in the range 10^{12} to 10^{19} s^{-1}. The entropy was negative up to $\alpha = 0.75$ but changed to positive at higher conversions implying likely disorderliness of final products compared to reactants. The calorific value of Ash (Fraxinus) wood sawdust was 18.3 MJ/kg which is comparable to other biomass.

Acknowledgments

The authors thank the Hazel Woodhams Memorial Fund, Gas Safety Trust, Boat Safety Scheme, and Katie Haines for sponsoring this work.

Funding

This work was supported by the Gas Safety Trust - UK;Boat Safety Scheme - UK;

References

Ahmad, M. S., M. A. Mehmood, O. S. Al Ayed, Y. Guangbin, H. Luo, M. Ibrahim, U. Rashid, I. A. Nehdi, and G. Qadir. 2017. Kinetic analyses and pyrolytic behavior of para grass (urochloa mutica) for its bioenergy potential. *Bioresource Technology* 224: Elsevier Ltd: 708–13. doi:10.1016/j.biortech.2016.10.090.

Alves, A., D. Maia, and L. C. De Morais. 2016. Kinetic parameters of red pepper waste as biomass to solid biofuel. *Bioresource Technology* 204: Elsevier Ltd: 157–63. doi:10.1016/j.biortech.2015.12.055.

Bamford, C. H., and C. F. H. Tipper. 1980. Comprehensive Chemical Kinetics: Reactions in the Solid State. *Comprehensive Chemical Kinetics* 22.

Brebu, M., and C. Vasile. 2010. Thermal degradation of lignin- a review. *Cellulose Chemistry and Technology* 44 (9):353–63.

Ceylan, S., and Y. Topcu. 2014. Pyrolysis kinetics of hazelnut husk using thermogravimetric analysis. *Bioresource Technology* 156: Elsevier Ltd: 182–88. doi:10.1016/j.biortech.2014.01.040.

Ceylan, S., Y. Topcu, and Z. Ceylan. 2014. Thermal behaviour and kinetics of alga polysiphonia elongata biomass during pyrolysis. *Bioresource Technology* 171 (1): Elsevier Ltd: 193–98. doi:10.1016/j.biortech.2014.08.064.

Ch, T. S., S. D. Genieva, A. S. Dimitrova, and L. T. Vlaev. 2008. Non-isothermal degradation kinetics of filled with rise husk ash polypropene composites. *Express Polymer Letters* 2 (2):133–46. doi:10.3144/expresspolymlett.2008.18.

Chen, D., D. Liu, H. Zhang, Y. Chen, and L. Qian. 2015a. Bamboo pyrolysis using TG-FTIR and a lab-scale reactor: Analysis of pyrolysis behavior, product properties, and carbon and energy yields. *Fuel* 148: Elsevier Ltd: 79–86. doi:10.1016/j.fuel.2015.01.092.

Chen, D., Z. Zheng, F. Kexin, Z. Zeng, J. Wang, and L. Mengting. 2015b. Torrefaction of biomass stalk and its effect on the yield and quality of pyrolysis products. *Fuel* 159: Elsevier Ltd: 27–32. doi:10.1016/j.fuel.2015.06.078.

Chen, D., J. Zhou, and Q. Zhang. 2014. Effects of heating rate on slow pyrolysis behavior, kinetic parameters and products properties of moso bamboo. *Bioresource Technology* 169: Elsevier Ltd: 313–19. doi:10.1016/j.biortech.2014.07.009.

Chong, Y. Y., S. Thangalazhy-Gopakumar, S. Gan, H. K. Ng, L.-Y. Lee, and S. Adhikari. 2017. Kinetics and mechanisms for co-pyrolysis of palm Empty Fruit Bunch Fibre (EFBF) with Palm Oil Mill Effluent (POME) sludge. *Energy & Fuels* acs.energyfuels: 7b00877. doi:10.1021/acs.energyfuels.7b00877.

Collard, F. X., and J. Blin. 2014. A review on pyrolysis of biomass constituents: Mechanisms and composition of the products obtained from the conversion of cellulose, hemicelluloses and lignin. *Renewable and Sustainable Energy Reviews* 38: Elsevier: 594–608. doi:10.1016/j.rser.2014.06.013.

Daood, S. S., S. Munir, W. Nimmo, and B. M. Gibbs. 2010. Char oxidation study of sugar cane bagasse, cotton stalk and pakistani coal under 1% and 3% oxygen concentrations. *Biomass and Bioenergy* 34 (3): Elsevier Ltd: 263–71. doi:10.1016/j.biombioe.2009.10.014.

Ding, Y., O. A. Ezekoye, L. Shouxiang, and C. Wang. 2016. Thermal degradation of beech wood with thermogravimetry/fourier transform infrared analysis. *Energy Conversion and Management* 120: Elsevier Ltd: 370–77. doi:10.1016/j.enconman.2016.05.007.

Gu, X., C. Liu, X. Jiang, M. Xu, L. Lixian, K. Cheng, and L. Zhongzheng. 2014. Thermal behavior and kinetics of the pyrolysis of the raw/steam exploded poplar wood sawdust. *Journal of Analytical and Applied Pyrolysis* 106:177–86. doi:10.1016/j.jaap.2014.01.018.

Haykiri-Acma, H., S. Yaman, and S. Kucukbayrak. 2016. "Combustion characteristics of torrefied biomass materials to generate power." In *2016 4th IEEE International Conference on Smart Energy Grid Engineering, SEGE 2016*, 226–30. doi:10.1109/SEGE.2016.7589530.

Islam, M. A., M. Asif, and B. H. Hameed. 2015. Pyrolysis kinetics of raw and hydrothermally carbonized karanj (pongamia pinnata) fruit hulls via thermogravimetric analysis. *Bioresource Technology* 179: Elsevier Ltd: 227–33. doi:10.1016/j.biortech.2014.11.115.

Jeguirim, M., J. Bikai, Y. Elmay, L. Limousy, and E. Njeugna. 2014. Thermal characterization and pyrolysis kinetics of tropical biomass feedstocks for energy recovery. *Energy for Sustainable Development* 23: International Energy Initiative. Published by Elsevier Inc: 182–93. doi:10.1016/j.esd.2014.09.009.

Khawam, A., and D. R. Flanagan. 2006. Solid-state kinetic models: Basics and mathematical fundamentals. *Journal of Physical Chemistry B* 110 (35):17315–28. doi:10.1021/jp062746a.

Koyuncu, T., and Y. Pinar. 2007. The emissions from a space-heating biomass stove. *Biomass and Bioenergy* 31 (1):73–79. doi:10.1016/j.biombioe.2006.06.014.

Manaila, E., M. D. Stelescu, G. Craciun, and D. Ighigeanu. 2016. Wood sawdust/natural rubber ecocomposites cross-linked by electron beam irradiation. *Materials* 9 (7):1–23. doi:10.3390/ma9070503.

Mishra, G., J. Kumar, and T. Bhaskar. 2015. Kinetic studies on the pyrolysis of pinewood. *Bioresource Technology* 182: Elsevier Ltd: 282–88. doi:10.1016/j.biortech.2015.01.087.

Peter, M. 2002. Energy production from biomass (part 1): Overview of biomass. *Bioresource Technology journal* 83 (July 2001):37–46.

Singh, Y. D., P. Mahanta, and U. Bora. 2017. Comprehensive characterization of lignocellulosic biomass through proximate, ultimate and compositional analysis for bioenergy production. *Renewable Energy* 103: Elsevier Ltd: 490–500. doi:10.1016/j.renene.2016.11.039.

Skoulou, V., and A. Zabaniotou. 2007. Investigation of agricultural and animal wastes in greece and their allocation to potential application for energy production. *Renewable and Sustainable Energy Reviews* 11 (8):1698–719. doi:10.1016/j.rser.2005.12.011.

Slopiecka, K., P. Bartocci, and F. Fantozzi. 2012. Thermogravimetric analysis and kinetic study of poplar wood pyrolysis. *Applied Energy* 97: Elsevier Ltd: 491–97. doi:10.1016/j.apenergy.2011.12.056.

Sonobe, T., and N. Worasuwannarak. 2008. Kinetic analyses of biomass pyrolysis using the distributed activation energy model. *Fuel* 87 (3):414–21. doi:10.1016/j.fuel.2007.05.004.

Starink, M. J. 2003. The determination of activation energy from linear heating rate experiments: A comparison of the accuracy of isoconversion methods. *Thermochimica Acta* 404 (1–2):163–76. doi:10.1016/S0040-6031(03)00144-8.

Tian, L., B. Shen, X. Huan, L. Fukuan, Y. Wang, and S. Singh. 2016. Thermal behavior of waste tea pyrolysis by TG-FTIR analysis. *Energy* 103: Elsevier Ltd: 533–42. doi:10.1016/j.energy.2016.03.022.

Toufiq, R. M., M. Wei Yan, J. G. Helal Uddin, L. S. Kent Hoekman, C. J. Coronella, and V. R. Vásquez. 2013. Reaction kinetics of hydrothermal carbonization of loblolly pine. *Bioresource Technology* 139: Elsevier Ltd: 161–69. doi:10.1016/j.biortech.2013.04.028.

Varma, A. K., and P. Mondal. 2016. Physicochemical characterization and pyrolysis kinetics of wood sawdust. *Energy Sources, Part A: Recovery, Utilization and Environmental Effects* 38 (17):2536–44. doi:10.1080/15567036.2015.1072604.

Vlaev, L., N. Nedelchev, K. Gyurova, and M. Zagorcheva. 2008. A comparative study of non-isothermal kinetics of decomposition of calcium oxalate monohydrate. *Journal of Analytical and Applied Pyrolysis* 81 (2):253–62. doi:10.1016/j.jaap.2007.12.003.

Vlaev, L. T., V. G. Georgieva, and S. D. Genieva. 2007. Products and kinetics of non – isothermal decomposition of vanadium (Iv) oxide compounds. *Journal of Thermal Analysis and Calorimetry* 88:805–12.

Vyazovkin, S., A. K. Burnham, J. M. Criado, L. A. Pérez-Maqueda, C. Popescu, and N. Sbirrazzuoli. 2011. ICTAC kinetics committee recommendations for performing kinetic computations on thermal analysis data. *Thermochimica Acta* 520 (1–2): Elsevier B.V.: 1–19. doi:10.1016/j.tca.2011.03.034.

Wang, X., H. Mian, H. Wanyong, Z. Chen, S. Liu, H. Zhiquan, and B. Xiao. 2016. Thermogravimetric kinetic study of agricultural residue biomass pyrolysis based on combined kinetics. *Bioresource Technology* 219: Elsevier Ltd: 510–20. doi:10.1016/j.biortech.2016.07.136.

White, J. E., W. James Catallo, and B. L. Legendre. 2011. Biomass pyrolysis kinetics: A comparative critical review with relevant agricultural residue case studies. *Journal of Analytical and Applied Pyrolysis* 91 (1): Elsevier B.V.: 1–33. doi:10.1016/j.jaap.2011.01.004.

Wu, D., M. Schmidt, X. Huang, and F. Verplaetsen. 2017. Self-ignition and smoldering characteristics of coal dust accumulations in O2/N2 and O2/CO2 atmospheres. *Proceedings of the Combustion Institute* 36 (2): Elsevier Inc.: 3195–202. doi:10.1016/j.proci.2016.08.024.